Vision, Modeling, and Visualization (2011)
Peter Eisert, Konrad Polthier, and Joachim Hornegger (Eds.)

Is it Necessary to Model the Matrix Degrading Enzymes for Simulating Tumour Growth?

A. Toma[1,2], A. Mang[1], T. A. Schütz[1,3], S. Becker[1,2] and T. M. Buzug[1]

[1]Institute of Medical Engineering, University of Lübeck, Lübeck, Germany
[2]Centre of Excellence for Technology and Engineering in Medicine (TANDEM), Lübeck, Germany
[3] Graduate School for Computing in Medicine and Life Sciences, University of Lübeck, Lübeck, Germany

Abstract

We propose a hybrid continuum–discrete model to simulate tumour growth on a microscopic scale. The lattice–based spatio–temporal model consists of reaction–diffusion equations that describe interactions between cancer cells and their microenvironment. The components that are typically considered are usually nutrients, like oxygen and glucose, matrix degrading enzymes (MDE) and the extracellular matrix (ECM).
The in–vivo processes are very complex and occur on different levels. This in turn leads to huge computational costs. Thus, the aim is to describe the processes on the basis of simplified mathematical approaches, which depict realistic results at the same time. In this work we discuss if we have to model the MDEs or if the ECM can be modelled directly depending on the cancer cells distribution. Comparing the results for modelling the tumour growth with the common choice and with the simplified model without MDE, we observe almost similar results. The model without MDE allows for a straightforward, fast and accurate implementation.

Categories and Subject Descriptors (according to ACM CCS): I.6.5 [Simulation and Modeling]: Model Development—Modeling methodologies

1. Introduction

Cancer is one of the most common diseases in adulthood and has gained more and more attention in research of different scientific disciplines in recent years.

Generally, the modelling of tumour growth is described either on a macroscopic [KCM*10], a microscopic [KTI*00, RA10] or a molecular level [AMD05], rarely multi-scale approaches are used. The macroscopic models are generally based on continuous, deterministic reaction-diffusion formalisms [KCM*10] and lead to a global description of the tumour as it can typically be observed in magnetic resonance imaging or computed tomography. Such model, though allowing for visual comparisons with medical, non-invasive in-vivo imaging data, neglects the complex processes on the microscopic and molecular level. Mathematical approaches for simulating tumour growth on the cellular level are typically formulated in terms of discrete methods like cellular automata [HD08, FMV02] or agent based models [CUD10, DSCH09].

The main core for simulation methods is the simplification of the underlying complex processes while maintaining the realistic findings. One of the most important approaches for modelling cell processes was proposed from Anderson and Chaplain in 1998 [AC98] where the discretisation of partial differential equations gives a probability range for cells to move in a specific direction or in some cases to be quiescent. For modelling interactions between cancerous cells, the extracellular matrix (ECM) and matrix degrading enzymes (MDE) it is common to use a system of partial differential equations that describe the haptotactic and/or chemotactic movement of the cells [AGL*10, And05, ARGQ09, GC08, JQC10]. For the ECM the equation consists of a degrading and a remodelling term. Degradation occurs where the enzymes are located, hence the first part of the ECM depends on the MDE. It has been proven that the degradation of the ECM occurs because the MDEs are secreted by tumour cells [lTM01]. As described above, mathematical modelling provides for simplifying the very complex real processes. To this end we introduce a model describing the same processes as above, without explicitly modelling MDE. That is the degradation of the ECM modelled without the specific

DOI: 10.2312/PE/VMV/VMV11/361-368

term of the matrix degrading enzymes. We assume in our implementation that the cancer cells themselves are able to degrade the matrix. To get similar results, we determine the level of the degradation on the basis of the degrading parameter α_f. To prove the findings, we compare the two models by simulating different initial conditions for the ECM and by different arrangements of the nutrient delivering blood vessels. In this work we neglect the cell-cell adhesion of cancerous cells to better focus on the influence of the MDEs and matrix.

In this paper, we aim to simplify the mathematical modelling of the complex biological processes. In section 2, we study the common method for cellular interactions described by eq. (1) and the simplest possible case of it is described in equation (2). Finally, in Section 3, we discuss our results for different positions of capillaries and for a random or constant distributed extracellular matrix, highlighting the successes of our approach. In section 4 we conclude with a short outlook.

2. Methods

We simulate brain tumour growth on a two-dimensional area of brain tissue $\Omega = [0,1] \times [0,1]$ with boundary $\Gamma := \partial\Omega$. A 400×400 grid with a space step of h = 0.0025 is overlaid forming the basis for the discrete methods. The domain we consider is defined in a region of 4 mm $\times$ 4 mm, thus each square of the grid corresponds approximately to the area of a tumour cell, i.e. $6.25 \times 10^{-6}\,\mathrm{cm}^2$ (cf. [And05]). The grid is introduced for computed tumour or necrotic cells but not for the host tissue considered, because of the clumps like growth of the tumour. For interactions of the tumour with the host tissue, we recommend to look at the macroscopic scale [MBT*11, BMT*10]. At this level one gets a better representation of processes like the displacement and deformation of the environmental tissue.

2.1. Hybrid Model

As for the description of the tumour growth, we use a hybrid model [And05], i.e. the model includes continuous and discrete methods. The complete system of equations consisting of the distribution of cancer cells c, nutrients concentration u, ECM f and MDE m is given by:

$$\frac{\partial c}{\partial t} = D_c \nabla^2 c - \chi \nabla \cdot (c \nabla u) - \rho \nabla \cdot (c \nabla f), \tag{1a}$$

$$\frac{\partial u}{\partial t} = D_u \nabla^2 u - \alpha_u u, \tag{1b}$$

$$\frac{\partial f}{\partial t} = -\alpha_f f m + \beta_f f, \tag{1c}$$

$$\frac{\partial m}{\partial t} = D_m \nabla^2 m + \beta_m c - \alpha_m m, \tag{1d}$$

where D_c, D_u and D_m denote the diffusion coefficients of the tumour cell, oxygen and enzymes, respectively. Furthermore, χ is the chemotaxis coefficient and ρ the haptotaxis coefficient. Uptake and decay of particular substances due to tumour growth are α_u and α_f (uptake rate for glucose and ECM) and α_m (decay coefficient for MDE). β_f and β_m represent the remodelling parameter for ECM and the productions constant for MDE, respectively.

For our new model we assume that the extracellular matrix is directly affected by the cancerous tissue i.e. we unify (1c) and (1d) such as to model solely the ECM. The only change we made in this model is the first component of the ECM equation, i.e. from $-\alpha_f f m$ to $-\alpha_f f c$. The complete system is now defined as follows:

$$\frac{\partial c}{\partial t} = D_c \nabla^2 c - \chi \nabla \cdot (c \nabla u) - \rho \nabla \cdot (c \nabla f), \tag{2a}$$

$$\frac{\partial u}{\partial t} = D_u \nabla^2 u - \alpha_u u, \tag{2b}$$

$$\frac{\partial f}{\partial t} = -\alpha_f f c + \beta_f f. \tag{2c}$$

Due to the diffusive behaviour of the MDEs, we regulate the uptake of the extracellular matrix through the varying parameter α_f. Both models are initialized in the same way: 100 tumour cells are placed in the middle of the domain. As for the ECM we refer to section 2.3. The amount of initially available nutrients (Fig. 1, left image) are estimated from the steady state solution of (1b)/(2b). The distribution of the nutrients over time is shown in Fig. 1, right image. The initial MDE concentration is set to zero throughout the domain. Depending on the location of the blood vessels, we have Dirichlet and Neumann boundary conditions (see sec. 2.3). For the ECM and MDE we assume zero flux boundary conditions.

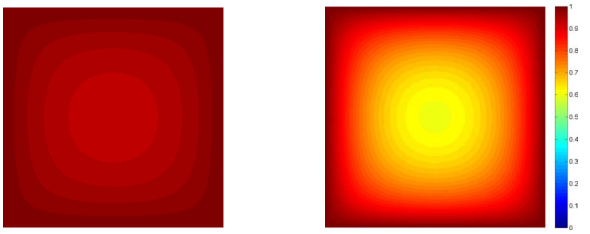

Figure 1: *The distribution of the nutrients with blood vessels at all surrounding sides at time t=0 (left) and 335 h (right). Colouration as given in the look-up table.*

2.2. Non-dimensionalisation

We rescale and non-dimensionalise the variables and parameters of the systems (1) and (2) so that all computed quantities are of similar magnitude in the range $[0,1]$. The new

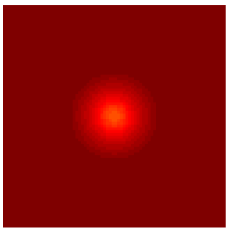

(a) modelled with (1), t=100h

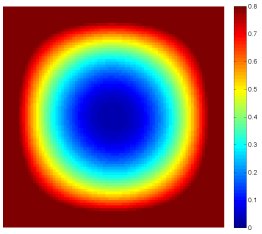

(b) modelled with (1), t=325h

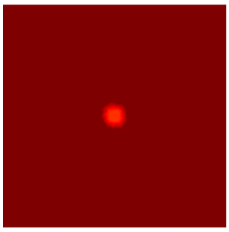

(c) modelled with (2), t=100h

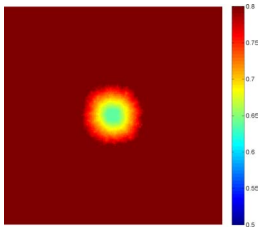

(d) modelled with (2), t=325h

Figure 2: *The distribution of the ECM with constant initial condition modelled with method (1) and (2) at time t=100 h (left), 335 h (right). Colouration as given in the look-up table.*

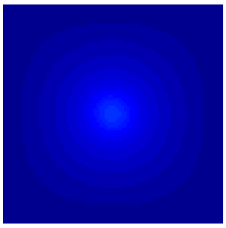

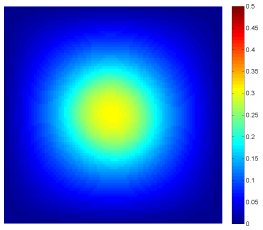

Figure 3: *The distribution of the MDE at time t=100 h (left) and 335 h (right). Colouration as given in the look-up table.*

dimensionless variables are defined as:

$$\hat{x} = \frac{x}{L}, \quad \hat{t} = \frac{t}{\tau}, \quad \hat{c} = \frac{c}{c_0},$$
$$\hat{u} = \frac{u}{u_0}, \quad \hat{f} = \frac{f}{f_0}, \quad \hat{m} = \frac{m}{m_0}. \tag{3}$$

For the appropriate length scale L we use 0.1 cm (taken from [AGL*10, GC08]), for the time $\tau = L^2/D$, where $D = 10^{-6}\,\mathrm{cm}^2/\mathrm{s}$ is a representative diffusion coefficient (c.f. [GC08]). For the tumour cell density c_0, the nutrient concentration u_0 and ECM density f_0 we follow [And05], the matrix degrading enzyme density $m_0 = 0.1\,\mathrm{nM}$ is taken from [AGL*10].

For the dimensionless cell diffusion coefficient of the tumour cells we get $\hat{D}_c = \frac{\tau D_c}{L^2} = 10^{-5}$ and for the dimensionless haptotaxis parameter $\hat{\rho} = \frac{\tau\rho f_0}{L^2} = 0.26$ [And05, GC08].

We assume the chemotaxis parameter χ to be equal to the haptotaxis parameter, so the cells are equally attracted to nutrients and interacting with the ECM. The parameter $D_u = 10^{-5}\,\mathrm{cm}^2/\mathrm{s}$ is taken from [And05], so we get $\hat{D}_u = \frac{\tau D_u}{L^2} = 10$. The uptake rate is assumed to be $\hat{\alpha}_u = \frac{\tau c_0 \alpha_0}{u_0} = 6.25 \cdot 10^{-5}$. The parameters of the MDE, $\hat{\beta}_m = 1$ and $\hat{\alpha}_m = 0$ are taken from [And05]. The dimensionless diffusion coefficient of the MDE is assumed to be 0.08. For the ECM uptake and the remodelling part we choose different parameters for system (1) and for (2). For the MDE dependent model, we follow [SRML09]. Apart from that we assume for the constants $\hat{\alpha}_f = 0.01$ and $\hat{\beta}_f = 0.001$ because of the differences of MDE and cancer. Hence, we drop the hats in the following for notational convenience.

2.3. Numerical Implementation

For discretising the systems of partial differential equations (1) and (2) we use standard finite-difference and the finite element method. For equations (1a) and (2a), respectively, we use the resulting coefficients of the five- and nine-point finite-difference stencil to generate the probabilities of the movement of an individual cell in response to its local milieu. The 5-point stencil is equivalent to the von Neumann neighbourhood and the 9-point stencil to the Moore neighbourhood. We implement both and use a switching mechanism to select one of them for each iteration (see section 2.5). With $t = mk$, $x = ih$ and $y = jh$ (m , k, i, j, $h > 0$) we use forward differences at time point t_m and second order central differences for the spatial derivative at point $x_{i,j}$. The resulting equation for the 5-point stencil governing the chemotactic-haptotactic migration of the tumour cell (1a) and (2a) has then the form

$$c_{i,j}^{m+1} = P_0 \cdot c_{i,j}^m + P_1 \cdot c_{i+1,j}^m + P_2 \cdot c_{i-1,j}^m + P_3 \cdot c_{i,j+1}^m + P_4 \cdot c_{i,j-1}^m,$$

where P_0 is proportional to the quiescent cells. P_1, P_2, P_3, P_4 are probabilities that are proportional to a movement of the cell to the right, left, up or down, respectively. For the 9-point stencil, the resulting equations are straight forward, we just have additionally the probabilities P_5, P_6, P_7, P_8, which are proportional to a movement of the cell to the bottom right, bottom left, top right and top left, respectively. For the computation of the nutrients (1b), (2b) and MDE (1d) we use the method of finite elements. Because of the discrete-continuum interaction in every time step, we have to solve the equations in the steady state. The boundary and initial conditions for nutrients depend on their position relative to the oxygen and glucose delivering blood vessels or capillaries. This can be modelled by placing them at all four surrounding boundaries, at two of them, or on a single side only. For the sites occupied by blood vessels we apply Dirichlet boundary conditions with constant functions. For the remaining boundaries we use zero flux boundary conditions

(Neumann). Thus at any time $t \in [0,T]$

$$\partial u/\partial n = 0 \qquad \text{on } \Gamma_N,$$
$$u = u_d \qquad \text{on } \Gamma_D,$$

where Γ_N and Γ_D are the Neumann and Dirichlet boundary, respectively, with $\Gamma_N \cup \Gamma_D = \Gamma$. We set $u_d = 1$ since the concentration of glucose and oxygen is highest in the capillaries. For the extracellular matrix we model different initial conditions. On one side we take random values between 0 and 1, which corresponds to the density of the ECM following [And05]. On the other side we take a constant value $f(x) = 0.8$ to allow for the assumption that the density of the ECM is high at the beginning, but smaller than 1, which would be equivalent to a maximum of density. Fig. 2 depicts the distribution of the ECM with a constant initial condition modelled in dependency of the MDE (Fig. 2(a), 2(b)) and with the method (2), (Fig. 2(c), 2(d)). This choice of value is taken in reference to [Zam05], where the extracellular space is described.

2.4. Cell actions

For modelling the cell actions proliferation, motility, death and quiescent we have to look at some criteria. In each time step and for each tumour cell we account for the local nutrient concentration and decide then how the cell will react. In case that the oxygen value is under a critical threshold $a_{crit} = [0.2, 0.6]$, we assume that with a probability of 80% the cell will die due to insufficient oxygen. Thus, the cell consequently is marked as necrotic tissue and not considered for the next step. After checking the necrosis criteria, each cell moves according to the scheme described in section 2.3. In case the nutrient concentration is high enough, the cell is selected to divide. The duration of the proliferation takes some hours, in general a day [AMD05]. We assume that the cell cycle takes eight hours, which is realistic for malignant tumours [And05]. In case there is no free place in the neighbourhood, the tumour cell becomes quiescent until a free place becomes available or the cell becomes necrotic due to insufficient oxygen.

2.5. Neighbourhood and Update

For lattice-based models the update of the state of an individual cell is computed on the basis of its local neighbourhood. We use a 50/50 probability to decide if we take the eight neighbours into account or the four orthogonally surrounding cells [TMS*11]. At each discrete time point and for each cell in order to decide whether the Moore or the von Neumann neighbourhood is favoured, we generate a random number.

Additionally, cells are not updated in a left-to-right, top-to-bottom manner but randomly [And05]. If we would run sequentially over the lattice to look at every tumour cell one by one, the first cell has almost always more possibilities for migration (in case of division: to place the daughter cells) than the one sitting very next to it.

3. Results and Discussion

For all simulations we show the progression of the extracellular matrix, the nutrient distribution, the tumour cell arrangement and additionally in case method (1) is used the matrix degrading enzymes. We show all results after 200 and 640 iteration steps, which is equivalent to a period of time of 100 h and 325 h, respectively. At first computer simulations using system (1) have been run assuming a random initial ECM distribution (see also sec. 2.3). Corresponding results are shown in Fig. 4. We compared these data with the simulation results of system (2), i.e. without explicitly modelling the MDE (Fig. 5), but using the same initial conditions. Obviously expected differences for the ECM in the Fig. 4(a) and 5(a) can be observed, since the degradation is modelled differently. The extracellular matrix in Fig. 4(a) has been reduced through the diffusive MDEs shown in Fig. 4(c). This is because the parameter α_f has been chosen to be smaller than the one in model (1).

Comparing the tumour cell distribution in the Fig. 4(d), (h) and 5(c), (f), respectively, a quite similar size of the bulk can be observed. This becomes even more evident in Fig. 6 representing the difference image of the tumour cell distribution from Fig. 4(h) and 5(f). Apart from a small rim, only zero entries occur. The points with values 1 and -1 show the missing tumour cells in one of the pictures, the entries between these values denote different states of the cancerous cell (proliferating, quiescent, necrotic). It should be noted that this must not be misunderstood as a qualitative difference error estimation because of the probabilities and randomly-guided model (see sec. 2).

We now vary the placement of the blood vessels and initial condition for the ECM into a constant value to evaluate the above statement. Fig. 7 shows the results simulated with Dirichlet and Neumann boundary conditions, i.e. the capillaries are placed at two sides, at the top and at the bottom of the domain. Contrary, Fig. 8 shows results modelled with the second approach (2). Again, we notice a quite similar structure of the tumour 7(d), (h) and comparing 8(c), (f). However, the invasive spatial expansion of the cancerous cells are even better noticeable in Fig. 8(c) and (f). After 100 hours the tumour becomes a little bit more spherical using the second method (cf. Fig. 8(f)), but after 225 h a substantial proliferation towards the nutrients delivering vessels can be observed (cf. Fig. 8(f)). Here, we gain quite equal results for the cancer cells. We can also observe that the ECM in the Fig. 8(a) is at first just a little degraded compared to Fig. 7(a), because of the strong diffusion of the MDE. However, after 325 hours the distribution of the extracellular matrix in Fig. 8(d) manifests similar to the tumour in Fig. 8(f). These observations are also true for Fig. 9 and 10 where we assume nutrients delivering blood vessel at only one side. This can

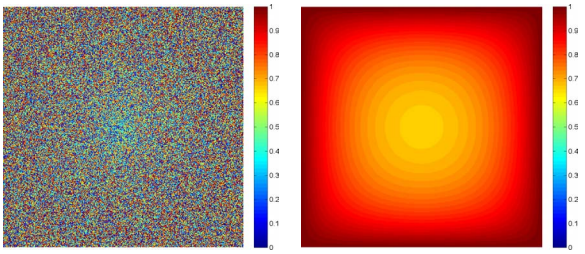

(a) ECM (b) nutrients

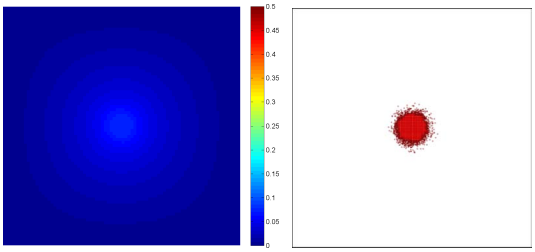

(c) MDE (d) tumour

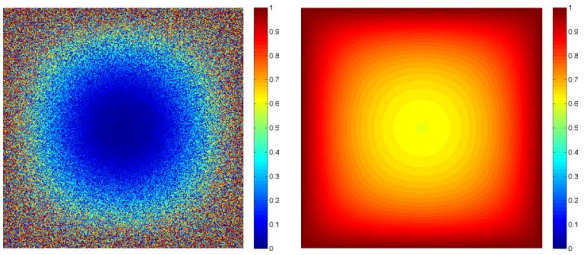

(e) ECM (f) nutrients

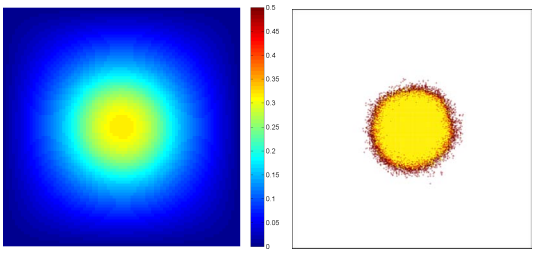

(g) MDE (h) tumour

Figure 4: *Results of method (1) at time t=100 h (a-d) and t=325 h (e-h), respectively. The initial condition of the ECM is a random distribution (see sec. 2.3), the blood vessels are placed at all surrounding sides. Colouration as given in the look-up table. For the cancerous cells yellow represents necrotic tissue, red quiescent cells and dark red proliferating and migrating cells.*

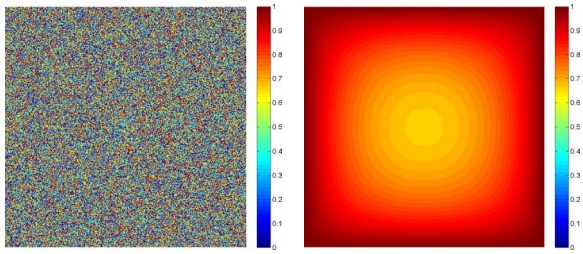

(a) ECM (b) nutrients

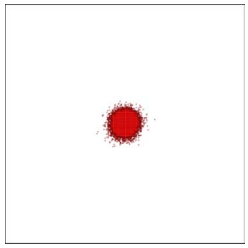

(c) tumour

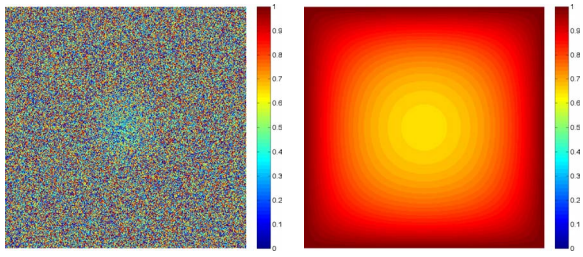

(d) ECM (e) nutrients

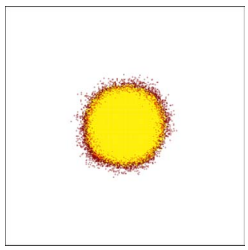

(f) tumour

Figure 5: *Results of method (2) at time t=100 h (a-c) and t=325 h (d-f), respectively. The initial condition of the ECM is random distribution (see sec. 2.3), the blood vessels are placed at all surrounding boundaries. Colouration as given in Fig. 4.*

be understood as an indicator for the potential of the second method to be used as a realistic description of the tumour without modelling the MDE explicitly.

As for the computational complexity of the two employed models, the proposed model (2) takes about 2.5 less time compared to model (1) in case the ECM is initialized with a random distribution (cf. Table 1). This gain in run-time does even increase to a factor of about 4.6 in case the ECM is initialized to a constant value. Simulations have been computed

using a single-threaded MATLAB implementation and have been run on a Pentium i7920 with 2.67 GHz and 12 GB of RAM.

initial ECM	capillaries	model 1	model 2
random	all sides	85	32
	two sides	125	48
	one side	138	61
constant	all sides	92	28
	two sides	133	31
	one sides	151	24

Table 1: *Computation time in minutes for the two models at different configurations.*

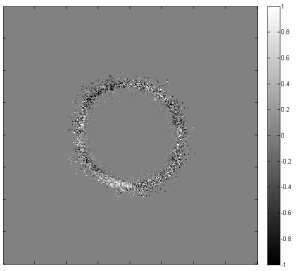

Figure 6: *Difference image of the tumour cell distributions computed with the two described methods.*

4. Conclusion and Outlook

This paper is devoted to the modelling of cellular processes of tumour cells, which is itself part of a complex system and the availability of efficient means therefore an essential prerequisite for modelling tumour growth. To this end we developed a novel lattice based approach that does not only provide a significant simplification compared to previous models but is also computationally efficient. This is achieved via unifying two partial differential equations allowing for a straightforward, fast and accurate implementation. Comparing the results for modelling haptotactic-chemotactic cancer growth using the common choice of the environment and the above introduced exclusion of the MDE, we observe a rather similar size of the tumour. The shape of the cancer modelled with the novel introduced method shows a more diffusive character, i.e. the cells are migrating farther from the bulk, constituting the high malignancy of the tumour. This diffuse tumour behaviour is very characteristic for this type of cancer as it has already been shown for in-vitro experiments [lTM01]. Faced with the requirement of modelling much more complex processes than the degradation of the ECM through the MDE (in order to adequately model tumour growth) the proposed model provides a reasonable trade-off between complexity and accuracy. Prospectively, it will also be essential to extend the devised model by cell-cell interactions and by incorporating the immune system [MP06] for a more realistic description of the in-vivo processes. In this case, the established efficiency gain, might pay off even more through alternative numerical solvers than the implemented finite element method. Further, as stated above, we aim at devising multi-scale tumour growth models that not only account for cell-cell interaction but also for molecular events as well as for information available from the macro-environment.

Acknowledgements A.T. and S.B. are financially supported by the European Union and the State Schleswig-Holstein (Program for the Future–Economy: 122-09-024). T.A.S. is supported by the Graduate School for Computing in Medicine and Life Sciences funded by Germanys Excellence Initiative [DFG GSC 235/1].

References

[AC98] ANDERSON A., CHAPLAIN M.: Continuous and discrete mathematical models of tumor-induced angiogenesis. *Bulletin of Mathematical Biology 60* (1998), 857–900. 1

[AGL*10] ANDASARI V., GERISCH A., LOLAS G., SOUTH A., CHAPLAIN M.: Mathematical modeling of cancer cell invasion of tissue: biological insight from mathematical analysis and computational simulation. *J. Math. Biol. DOI 10.1007/s00285-010-0369-1* (2010). 1, 3

[AMD05] ATHALE C., MANSURY Y., DEISBOECK T. S.: Simulating the impact of a molecular decision-process on cellular phenotype and multicellular patterns in brain tumors. *J of Theor Biol 233* (2005), 469–481. 1, 4

[And05] ANDERSON A.: A hybrid mathematical model of solid tumour invasion: the importance of cell adhesion. *Math. Med. Biol. Vol. 22 (2)* (2005), pp. 163–186. 1, 2, 3, 4

[ARGQ09] ANDERSON A., REJNIAK K., GERLEE P., QUARANTA V.: Microenvironment driven invasion: a multiscale multimodel investigation. *J. Math. Biol. 58* (2009), 579–624. 1

[BMT*10] BECKER S., MANG A., TOMA A., SCHÜTZ T., BUZUG T.: In-silico oncology: An approximate model of brain tumor mass effect based on directly manipulated free form deformation. *Int. J. Comput. Assist. Radiol. Surg. 5* (2010), 607–622. 2

[CUD10] CHEN L. L., ULMER S., DEISBOECK T. S.: An agent-based model identifies mri regions of probable tumor invasion in a patient with glioblastoma. *Phys. Med. Biol. 55* (2010), 329–338. 1

[DSCH09] DRÉAU D., STANIMIROV D., CARMICHAEL T., HADZIKADIC M.: An agent-based model of solid tumor progression. *J. Bioinform. Comput. Biol. 5462* (2009), 187–198. 1

[FMV02] FERREIRA JUNIOR S., MARTINS M., VILELA M.: A reaction-diffusion model for the growth of avascular tumor. 1

[GC08] GERISCH A., CHAPLAIN M.: Mathematical modelling of cancer cell invasion of tissue: Local and non-local models and the effect of adhesion. *J. of Theor. Biol. 250* (2008), 684–704. 1, 3

[HD08] HATZIKIROU H., DEUTSCH A.: Cellular automata as microscopic models of cell migration in heterogeneous environments. *Curr. Top. Dev. Biol. doi:10.1016/S0070-2153(07)81014-3* (2008). 1

[JQC10] JEON J., QUARANTA V., CUMMINGS P.: An off-lattice hybrid discrete-continuum model of tumor growth and invasion. *Biophysical Journal 98* (2010), 37–47. 1

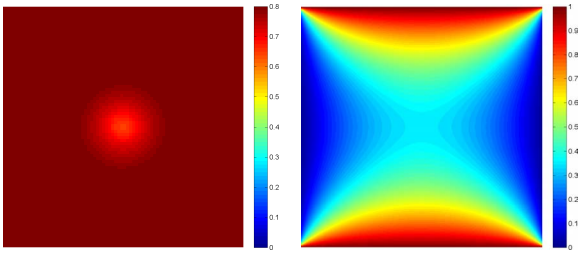

(a) ECM (b) nutrients

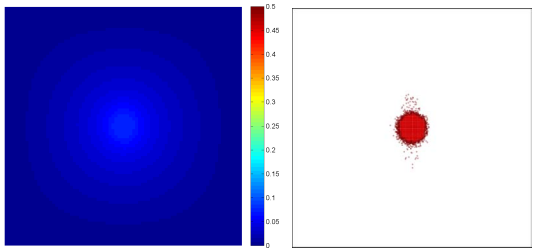

(c) MDE (d) tumour

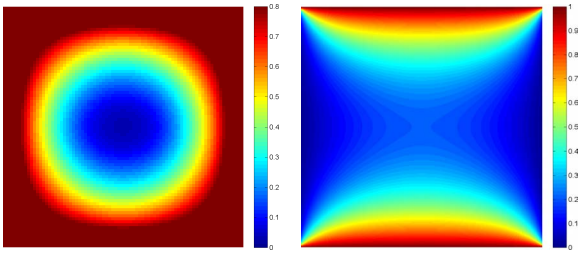

(e) ECM (f) nutrients

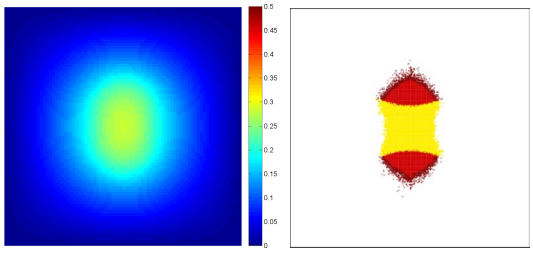

(g) MDE (h) tumour

Figure 7: *Results of method (1) at time t=100 h (a-d) and 335 h (e-h), respectively. The initial condition of the ECM is constant (see sec. 2.3), the blood vessels are placed at the top and bottom. Colouration as given in Fig. 4.*

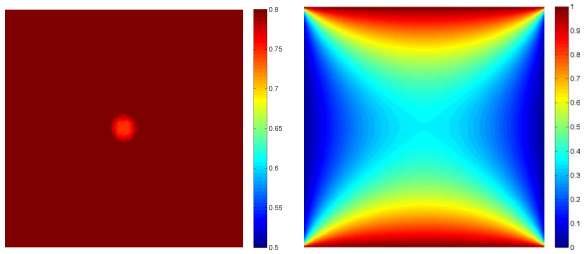

(a) ECM (b) nutrients

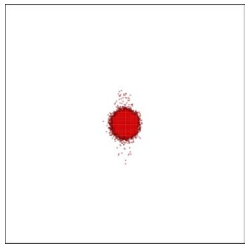

(c) tumour

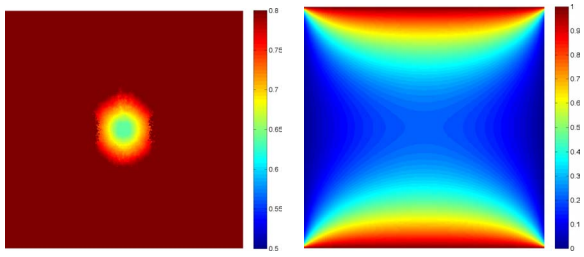

(d) ECM (e) nutrients

(f) tumour

Figure 8: *Results of method (2) at time t=100 h (a-c) and 335 h (d-f), respectively. The initial condition of the ECM is constant (see sec. 2.3), the blood vessels are placed at the top and bottom. Colouration as given in Fig. 4.*

[KCM*10] KONUKOGLU E., CLATZ O., MENZE B. H., STIELTJES B., WEBER M.-A., MANDONNET E., DELINGETTE H., AYACHE N.: Image guided personalization of reaction-diffusion type tumor growth models using modified anisotropic eikonal equations. *IEEE Transact. Med. Imaging. 29* (2010), 77–95. 1

[KTI*00] KANSAL A., TORQUATO S., IV G. H., CHIOCCA E., DEISBOECK T.: Cellular automaton of idealized brain tumor growth dynamics. *BioSystems 55* (2000), 119–127. 1

[ITM01] LGE TYSNES B. B., MAHESPARAN R.: Biological mechanisms of glioma invasion and potential therapeutic targets. *J. of Neuro-Oncology 53* (2001), 129–147. 1, 6

[MBT*11] MANG A., BECKER S., TOMA A., SCHÜTZ T., KÜCHLER J., TRONNIER V., BONSANTO M., BUZUG T.: A model of tumour induced brain deformation as bio-physical prior for non-rigid image registration. In *Int. Symp. on Biomed. Imaging* (2011), pp. 578–581. 2

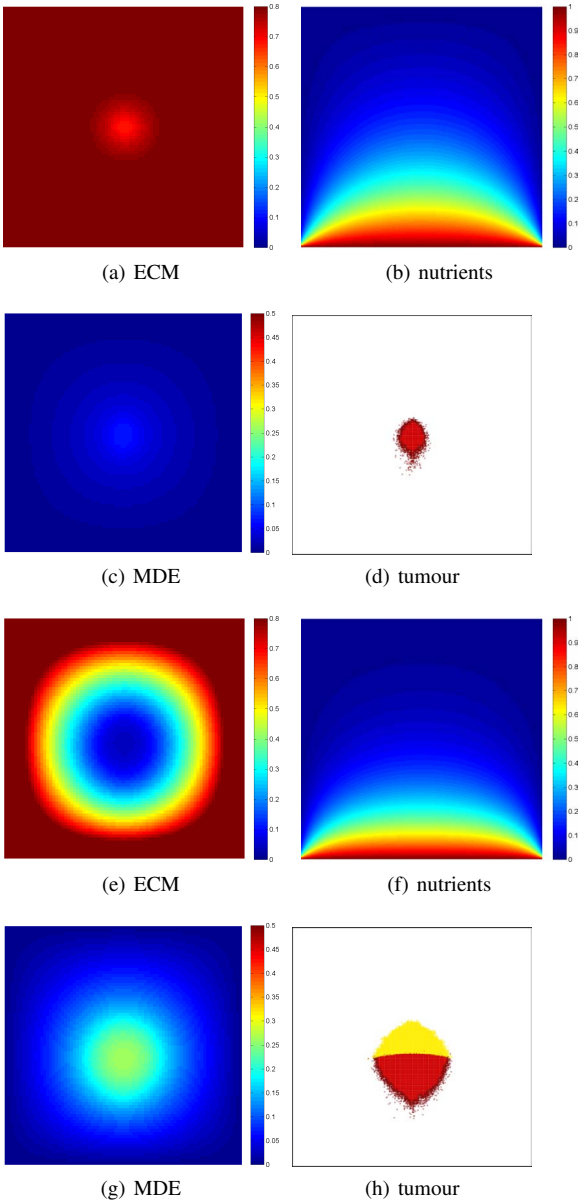

(a) ECM (b) nutrients

(c) MDE (d) tumour

(e) ECM (f) nutrients

(g) MDE (h) tumour

Figure 9: *Results of method (1) at time t=100 h (a-d) and 335 h (e-h), respectively. The initial condition of the ECM is constant (see sec. 2.3), the blood vessels are placed only at the top. Colouration as given in Fig. 4.*

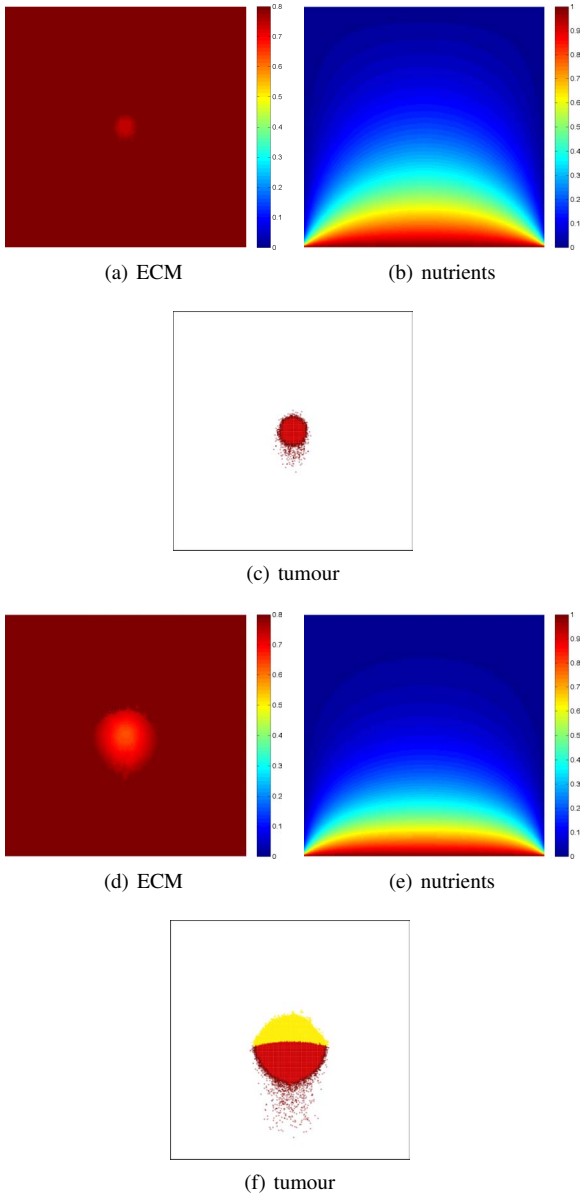

(a) ECM (b) nutrients

(c) tumour

(d) ECM (e) nutrients

(f) tumour

Figure 10: *Results of method (1) at time t=100 h (a-c) and 335 h (d-f), respectively. The initial condition of the ECM is constant (see sec. 2.3), the blood vessels are placed only at the top. Colouration as given in Fig. 4.*

[MP06] MALLET D., PILLIS L. D.: A cellular automata model of tumor-immune system interactions. *J Theor Biol 239* (2006), 334–350. 6

[RA10] REJNIAK K. A., ANDERSON A. R. A.: Hybrid models of tumor growth. *Wiley. Interdiscipl. Rev. Syst. Biol. Med. DOI: 10.1002/wsbm.102* (2010). 1

[SRML09] SZYMAŃSKA Z., RODRIGO C., M. LACHOWICZ M. C.: Mathematical modelling of cancer invasion of tissue: The rolle and effect of nonlocal interactions. *Math. Models Meth. Appl. Sci. 19 (2)* (2009), 257–281. 3

[TMS*11] TOMA A., MANG A., SCHÜTZ T., BECKER S., BUZUG T.: An efficient regular lattice approach for discrete modelling of tumour growth. In *Int. J. Comput. Assist. Radiol. Surg.* (2011). 4

[Zam05] ZAMECNIK J.: The extracellular space and matrix of gliomas. *Acta Neuropathol. 110* (2005), 435–442. 4